Chapter 17
Supracentrality Analysis of Temporal Networks with Directed Interlayer Coupling

Dane Taylor, Mason A. Porter, and Peter J. Mucha

Abstract We describe centralities in temporal networks using a supracentrality framework to study centrality trajectories, which characterize how the importances of nodes change with time. We study supracentrality generalizations of eigenvector-based centralities, a family of centrality measures for time-independent networks that includes PageRank, hub and authority scores, and eigenvector centrality. We start with a sequence of adjacency matrices, each of which represents a time layer of a network at a different point or interval of time. Coupling centrality matrices across time layers with weighted interlayer edges yields a *supracentrality matrix* $\mathbb{C}(\omega)$, where ω controls the extent to which centrality trajectories change with time. We can flexibly tune the weight and topology of the interlayer coupling to cater to different scientific applications. The entries of the dominant eigenvector of $\mathbb{C}(\omega)$ represent *joint centralities*, which simultaneously quantify the importances of every node in every time layer. Inspired by probability theory, we also compute *marginal* and *conditional centralities*. We illustrate how to adjust the coupling between time layers to tune the extent to which nodes' centrality trajectories are influenced by the oldest and newest time layers. We support our findings by analysis in the limits of small and large ω.

Keywords Temporal networks · Centrality · PageRank · Multilayer networks · Multiplex networks

D. Taylor (✉)
University of Wyoming, Laramie, WY, USA
e-mail: dane.taylor@uwyo.edu

M. A. Porter
University of California, Los Angeles, CA, USA
e-mail: mason@math.ucla.edu
Santa Fe Institute, Santa Fe, NM, USA

P. J. Mucha
Dartmouth College, Hanover, NH, USA
e-mail: peter.j.mucha@dartmouth.edu

17.1   Introduction

Quantifying the importances of nodes through the calculation of 'centrality' measures is a central topic in the study of networks (Newman 2018). It is important in numerous and diverse applications, including identification of influential people (Bonacich 1972; Faust 1997; Borgatti et al. 1998; Kempe et al. 2003), ranking web pages in searches (Brin and Page 1998; Page et al. 1999; Kleinberg 1999), ranking teams and individual athletes in sports (Callaghan et al. 2007; Saavedra et al. 2010; Chartier et al. 2011), identification of critical infrastructures that are susceptible to congestion or failure (Holme 2003; Guimerà et al. 2005), quantifying impactful judicial documents (Leicht et al. 2007; Fowler et al. 2007; Fowler and Jeon 2008) and scientific publications (Bergstrom et al. 2008), revealing drug targets in biological systems (Jeong et al. 2001), and much more.

Because most networks change with time (Holme and Saramäki 2012, 2013; Holme 2015), there is much interest in extending centralities to temporal networks (Liao et al. 2017). Past efforts have generalized quantities such as betweenness centrality (Tang et al. 2010; Kim et al. 2012; Alsayed and Higham 2015; Williams and Musolesi 2016; Fenu and Higham 2017), closeness centrality (Tang et al. 2010; Pan and Saramäki 2011; Kim et al. 2012; Williams and Musolesi 2016), Bonacich and Katz centrality (Lerman et al. 2010; Grindrod and Higham 2014), win/lose centrality (Motegi and Masuda 2012), communicability (Grindrod et al. 2011; Estrada 2013; Grindrod and Higham 2013; Chen et al. 2016; Arrigo and Higham 2017; Fenu and Higham 2017), dynamic sensitivity (Huang and Yu 2017), coverage centrality (Takaguchi et al. 2016), PageRank (Walker et al. 2007; Rossi and Gleich 2012; Mariani et al. 2015, 2016; You et al. 2017), and eigenvector centrality (Praprotnik and Batagelj 2015; Huang et al. 2017; Flores and Romance 2018). A common feature of these extensions is that they illustrate the importance of using methods that are designed explicitly for temporal networks, as opposed to various alternatives. These alternatives include aggregating a temporal network into a single 'time-independent' network, independently analyzing a temporal network at different instances of time, and binning a temporal network into time windows and analyzing those windows independently. With aggregation, it is not even possible to study centrality trajectories (i.e., how centralities change with time).

Because one can derive many centralities by studying walks on a network, some of the above temporal generalizations of centrality involve the analysis of so-called 'time-respecting paths' (Kossinets et al. 2008; Kostakos 2009). There are multiple ways to define a time-respecting path, including the possibility of allowing multiple edge traversals per time step for a discrete-time temporal network. There are also multiple ways to quantify the length of a time-respecting path (Williams and Musolesi 2016), because such a path can describe the number of edges that are traversed by a path, latency between the initial and terminal times of a path, or a combination of these ideas. It is necessary to make choices even to define a notion of a 'shortest path' (from which one can formulate several types of centrality). Consequently, some of

the diversity in the various temporal generalizations of centrality measures arises from the diversity in defining and measuring the length of a time-respecting path.

In the present work, we examine a notion of *supracentrality* (Taylor et al. 2017, 2021), which one can calculate by representing a temporal network as a sequence of network layers and coupling those layers to form a multilayer network (specifically, a multiplex network (Kivelä et al. 2014; Porter 2018)). See Fig. 17.1 for illustrative examples. The sequence of network layers, which constitute *time layers*, can represent a discrete-time temporal network at different time instances or a continuous-time network in which one bins (i.e., aggregates (Taylor et al. 2017)) the network's edges to form a sequence of time windows with interactions in each window. This approach is motivated by the use of a multiplex-network representation to detect communities in temporal networks through maximization of multilayer modularity (Mucha and Porter 2010; Bassett et al. 2013; Weir et al. 2017; Pamfil et al. 2019). There is also widespread interest in generalizing centrality measures to multilayer networks more generally (Magnani and Rossi 2011; Ng et al. 2011; De Domenico et al. 2013; Halu et al. 2013; Magnani et al. 2013; Solá et al. 2013; Battiston et al. 2014; Solé-Ribalta et al. 2014; Chakraborty and Narayanam 2016; Solé-Ribalta et al. 2016; Tavassoli and Zweig 2016; DeFord 2017; DeFord and Pauls 2017; Ding and Li 2018; Rahmede et al. 2017; Spatocco et al. 2018; Tudisco et al. 2018).

Our supracentrality framework generalizes a family of time-independent network centralities that are called *eigenvector-based* centralities, which are defined by the property of calculating centralities as the entries of an eigenvector (the so-called 'dominant' eigenvector) that corresponds to the largest-magnitude eigenvalue (the 'dominant' eigenvalue[1]) of a *centrality matrix* $C(\mathbf{A})$, which one defines by some function of a network's adjacency matrix $\mathbf{A}$. Different choices for the centrality matrix recover some of the most popular centrality measures, including eigenvector centrality (by using $C(\mathbf{A}) = \mathbf{A}$) (Bonacich 1972), hub and authority scores (by using $C(\mathbf{A}) = \mathbf{A}\mathbf{A}^T$ for hubs and $\mathbf{A}^T\mathbf{A}$ for authorities) (Kleinberg 1999), and PageRank (Page et al. 1999) (see Sect. 17.2.2). Given a discrete-time temporal network in the form of a sequence of adjacency matrices $\mathbf{A}^{(t)} \in \mathbb{R}^{N \times N}$ for $t \in \{1, \ldots, T\}$, where $A_{ij}^{(t)}$ denotes a directed edge from entity i to entity j in time layer t, examining supracentralities involves two steps:

1. Construct a supracentrality matrix $\mathbb{C}(\omega)$, which couples centrality matrices $C(\mathbf{A}^{(t)})$ of the individual time layers $t = 1, t = 2, t = 3, \ldots$
2. Compute and interpret the dominant eigenvector of $\mathbb{C}(\omega)$.

For a temporal network with N nodes and T time layers, $\mathbb{C}(\omega)$ is a square matrix of size $NT \times NT$. We require the set of nodes to be the same for all time layers. However, it is easy to accommodate the appearance and disappearance of nodes by including extra instances of the entities in layers in which they otherwise do not appear (but without including any associated intralayer edges). The parameter ω

---

[1] Technically, we study the eigenvector that is associated with the largest positive eigenvalue of an irreducible, nonnegative matrix. We assume that this eigenvalue has a larger magnitude than all other eigenvalues.
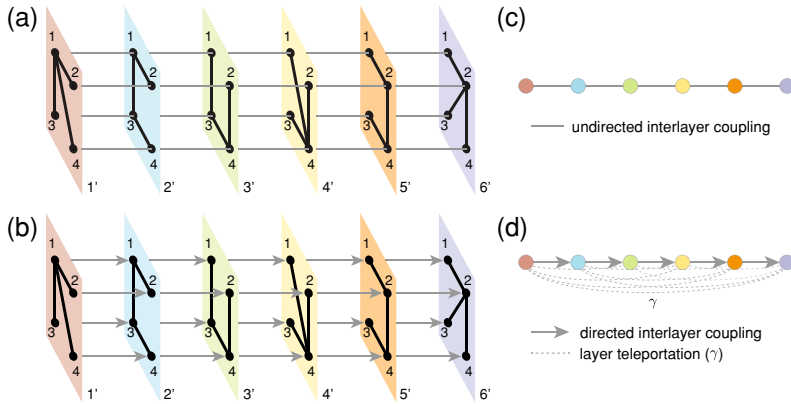
Fig. 17.1 Multiplex-network representations of a discrete-time temporal network. Given a temporal network with $N = 4$ nodes and $T = 6$ times, we represent the network at each time by a 'time layer' with adjacency matrix $\mathbf{A}^{(t)} \in \mathbb{R}^{N \times N}$ for $t \in \{1, \ldots, T\}$. **a, b** We represent the network as a multiplex network by coupling the layers with 'interlayer edges' (gray edges) that we encode in an interlayer-adjacency matrix $\tilde{A} \in \mathbb{R}^{T \times T}$. Panel **a** illustrates interlayer coupling in the form of an undirected chain, and panel **b** depicts directed coupling between layers. In panels **c** and **d**, we show visualizations of the networks that are associated with the matrix $\tilde{A}$ for panels **a** and **b**, respectively. In panel **d**, there are directed interlayer edges between consecutive time layers, so these interlayer edges respect the direction of time. Additionally, we construct connections of weight $\gamma > 0$ between corresponding nodes from all pairs of layers to ensure that $\tilde{A}$ corresponds to a strongly connected network, which in turn ensures that the centralities are positive and unique. By analogy to 'node teleportation' in PageRank (Gleich 2015), we refer to this coupling as 'layer teleportation'

scales the weights of the interlayer couplings to control the strength of the connection between time layers. It thus provides a 'tuning knob' to control how rapidly centrality trajectories can change with time.

An important aspect of the first step is that one chooses a topology to couple layers to each other. To do this, we define an interlayer-adjacency matrix $\tilde{A} \in \mathbb{R}^{T \times T}$, where the entry $\tilde{A}_{tt'}$ encodes the coupling from time layer t to time layer t'. In Fig. 17.1, we illustrate two possible choices for coupling the time layers. In the upper row, $\tilde{A} \in \mathbb{R}^{T \times T}$ encodes an undirected chain, which couples the time layers with *adjacent-in-time* coupling but neglects the directionality of time. In the lower row, by contrast, we couple the time layers with a directed chain that reflects the directionality of time. In addition to the directed, time-respecting edges, Fig. 17.1d also illustrates that we include weighted, undirected edges between corresponding nodes for all pairs of layers. This implements 'layer teleportation', which is akin to the well-known 'node teleportation' of the PageRank algorithm (Gleich 2015). Just like node teleportation, layer teleportation ensures that supracentralities are well-behaved (specifically, that they are positive and unique).

The second step to examine supracentralities involves studying the dominant right eigenvector of the supracentrality matrix $\mathbb{C}(\omega)$, which characterizes the *joint centrality* of each node-layer pair (i, t)—that is, the centrality of node i in time layer t—and thus reflects the importances of both node i and layer t. From the joint

centralities, one can calculate *marginal centralities* for only the nodes or only the time layers. One can also calculate *conditional centralities* that measure a node's centrality at time t relative only to the other nodes' centralities at time t. These concepts, which are inspired by ideas from probability theory, allow one to develop a rich characterization for how node centralities change with time.

In this chapter, we describe the supracentrality framework that we developed in Taylor et al. (2017, 2021) and extend these papers with further numerical explorations of how interlayer-coupling topology affects supracentralities. We apply this approach to a data set, which we studied in Taylor et al. (2017) and is available at Taylor (2019), that encodes the graduation and hiring of Ph.D. recipients between mathematical-sciences doctoral programs in the United States. We focus our attention on five top universities and examine how they are affected by the value of ω and the choice of $\tilde{A}$. Specifically, we compare the two strategies for interlayer coupling in Fig. 17.1 and explore the effect of reversing the directions of all directed edges. Our experiments reveal how to use ω and $\tilde{A}$ to tune the extent to which centrality trajectories of nodes are influenced by the oldest time layers, the newest time layers, and the direction of time.

17.2 Background Information

We now give some background information on multiplex networks and eigenvector-based centralities. Our supracentrality framework involves representing a temporal network as a multiplex network (see Sect. 17.2.1). In Sect. 17.2.2, we review eigenvector-based centrality measures.

17.2.1 *Analysis of Temporal Networks with Multiplex-Network Representations*

We study discrete-time temporal networks, for which we provide a formal definition.

Definition 17.1 (*Discrete-Time Temporal Network*) A *discrete-time temporal network* consists of a set $\mathcal{V} = \{1, \ldots, N\}$ of nodes and sets $\mathcal{E}^{(t)}$ of weighted edges that we index (using t) in a sequence of network layers. We denote such a network either by $\mathcal{G}(\mathcal{V}, \{\mathcal{E}^{(t)}\})$ or by the sequence $\{\mathbf{A}^{(t)}\}$ of adjacency matrices, where $A_{ij}^{(t)} = w_{ij}^t$ if $(i, j, w_{ij}^t) \in \mathcal{E}^{(t)}$ and $A_{ij}^{(t)} = 0$ otherwise.

As we illustrated in Fig. 17.1, we represent a discrete-time temporal network as a multiplex network with weighted and possibly directed coupling between the time layers. We restrict our attention to the following type of multiplex network.

Definition 17.2 (*Uniformly and Diagonally Coupled (i.e., Layer-Coupled) Multiplex Network*) Let $\mathcal{G}(\mathcal{V}, \{\mathcal{E}^{(t)}\}, \tilde{\mathcal{E}})$ be a T-layer multilayer network with node set

$\mathcal{V} = \{1, \ldots, N\}$ and interactions between node-layer pairs that are encoded by the sets $\{\mathcal{E}^{(t)}\}$ of weighted edges, where $(i, j, w_{ij}^t) \in \mathcal{E}^{(t)}$ if and only if there is an edge (i, j) with weight w_{ij}^t in layer t. The set $\tilde{\mathcal{E}} = \{(s, t, \tilde{w}_{st})\}$ encodes the topology and weights for coupling separate instantiations of the same node between a pair $(s, t) \in \{1, \ldots, T\} \times \{1, \ldots, T\}$ of layers. Equivalently, one can encode a multiplex network as a set $\{\mathbf{A}^{(t)}\}$ of adjacency matrices, such that $A_{ij}^{(t)} = w_{ij}^t$ if $(i, j, w_{ij}^t) \in \mathcal{E}^{(t)}$ and $A_{ij}^{(t)} = 0$ otherwise, along with an interlayer-adjacency matrix $\tilde{A}$ with entries $\tilde{A}_{st} = \tilde{w}_{st}$ if $(s, t, \tilde{w}_{st}) \in \tilde{\mathcal{E}}$ and $\tilde{A}_{st}^{(t)} = 0$ otherwise.

The coupling in Definition 17.2 is 'diagonal' because the only interlayer edges are ones that couple a node in one layer to that same node in another layer. It is 'uniform' because the coupling between two layers is identical for all nodes in those two layers. A multilayer network with both conditions is called 'layer-coupled' (Kivelä et al. 2014).

As we illustrated in Fig. 17.1, we focus our attention on two choices for coupling time layers:

(A) $\tilde{A}$ encodes an undirected chain:

$$\tilde{A}_{tt'} = \begin{cases} 1, & |t' - t| = 1 \\ 0, & \text{otherwise}; \end{cases} \tag{17.1}$$

(B) $\tilde{A}$ encodes a directed chain with layer teleportation:

$$\tilde{A}_{tt'} = \begin{cases} 1 + \gamma, & t' - t = 1 \\ \gamma, & \text{otherwise}, \end{cases} \tag{17.2}$$

where $\gamma > 0$ is the *layer-teleportation probability*. In Sect. 17.4, we compare the effects on centrality trajectories of these two choices of $\tilde{A}$.

17.2.2 Eigenvector-Based Centrality for Time-Independent Networks

Arguably the most notable—and certainly the most profitable—type of centrality is PageRank, which provided the mathematical foundation for the birth of the web-search algorithm of the technology giant Google (Brin and Page 1998; Page et al. 1999; Gleich 2015). PageRank quantifies the importances of the nodes of a network (e.g., a directed network that encodes hyperlinks between web pages) by computing the dominant eigenvector of the 'PageRank matrix' (i.e., 'Google matrix' (Langville and Meyer 2006))

$$\mathbf{C}^{(\text{PR})} = \sigma \mathbf{A}^T \mathbf{D}^{-1} + (1 - \sigma) N^{-1} \mathbf{1} \mathbf{1}^T, \tag{17.3}$$

where N is the number of nodes, $\mathbf{1} = [1, \ldots, 1]^T$ is a length-N vector of ones, and $\mathbf{A}$ is an adjacency matrix in which each entry A_{ij} encodes a directed (and possibly weighted) edge from node i to node j. The matrix $\mathbf{D} = \mathrm{diag}[d_1^{\mathrm{out}}, \ldots, d_N^{\mathrm{out}}]$ is a diagonal matrix that encodes the node out-degrees $d_i^{\mathrm{out}} = \sum_j A_{ij}$.

The PageRank matrix's dominant right eigenvector is a natural choice for ranking nodes, as it encodes a random walk's stationary distribution (which estimates the fraction of web surfers on each web page in the context of a web-search engine[2]). The term $\mathbf{A}^T \mathbf{D}^{-1}$ is a transition matrix that operates on column vectors that encode the densities of random walkers (Masuda et al. 2017). The term $N^{-1}\mathbf{1}\mathbf{1}^T$ is a *teleportation matrix*; it is a transition matrix of an unbiased random walk on a network with uniform all-to-all coupling between nodes. The *teleportation parameter* $\sigma \in (0, 1)$ implements a linear superposition of the two transition matrices and yields an irreducible matrix, even when the transition matrix $\mathbf{A}^T \mathbf{D}^{-1}$ is reducible. Because we introduced the concept of layer teleportation in Sect. 17.2.1, we henceforth refer to the traditional teleportation in PageRank as 'node teleportation'.

It is common to define the PageRank matrix as the transpose of Eq. (17.3); in that case, one computes the dominant left eigenvector instead of the dominant right eigenvector. However, we use the right-eigenvector convention to be consistent with a broader class of centrality measures called 'eigenvector-based centralities', in which one encodes node importances in the elements of the dominant eigenvector of some centrality matrix. In addition to PageRank, prominent examples of eigenvector-based centralities include (vanilla) eigenvector centrality (Bonacich 1972) and hub and authority (i.e., HITS) centralities (Kleinberg 1999). We now provide formal definitions.

Definition 17.3 (*Eigenvector-Based Centrality*)   Let $\mathbf{C} = C(\mathbf{A})$ be a centrality matrix, which we obtain from some function $C : \mathbb{R}^{N \times N} \mapsto \mathbb{R}^{N \times N}$ of the adjacency matrix $\mathbf{A}$, of a network $\mathscr{G}(\mathscr{V}, \mathscr{E})$. Consider the dominant right eigenvector $\mathbf{u}$, which satisfies

$$\mathbf{C}\mathbf{u} = \lambda_{\max}\mathbf{u}, \qquad (17.4)$$

where $\lambda_{\max} \in \mathbb{R}_+$ is the largest eigenvalue of $\mathbf{C}$. (This eigenvalue is guaranteed to be positive.) The ith entry u_i specifies the *eigenvector-based centrality* of node $i \in \mathscr{V}$ that is associated with the function C.

Definition 17.4 (*PageRank* (Page et al. 1999; Gleich 2015)) When $\mathbf{C}$ is given by Eq. (17.3), we say that Eq. (17.4) yields *PageRank centralities* $\{u_i^{(\mathrm{PR})}\}$.

Remark 17.1 It is also common to compute PageRank centralities from a left eigenvector (Gleich 2015). In the present chapter, we use a right-eigenvector formulation to be consistent with the other eigenvector-based centralities. One can recover the left-eigenvector formulation by taking the transpose of Eq. (17.4).

---

[2] PageRank has had intellectual impact well beyond web searches (Gleich 2015).

17.3   Supracentrality Framework

We now describe the supracentrality framework that we presented in Taylor et al.
(2021). The present formulation generalizes our formulation of supracentrality from
Taylor et al. (2017) that required interlayer coupling to take the form of an undirected
chain. (See the top row of Fig. 17.1.) To aid our presentation, we summarize our
mathematical notation in Table 17.1.

17.3.1   Supracentrality Matrices

We first describe a supracentrality matrix from Taylor et al. (2021).

Definition 17.5 (*Supracentrality Matrix*) Let $\{\mathbf{C}^{(t)}\}$ be a set of T centrality matri-
ces for a discrete-time temporal network with a common set $\mathcal{V} = \{1, \ldots, N\}$ of
nodes, and assume that $C_{ij}^{(t)} \geq 0$. Let $\tilde{A}$, with entries $\tilde{A}_{ij} \geq 0$, be a $T \times T$ interlayer-
adjacency matrix that encodes the interlayer couplings. We define a family of
supracentrality matrices $\mathbb{C}(\omega)$, which are parameterized by the interlayer-coupling
strength $\omega \geq 0$, of the form

$$\mathbb{C}(\omega) = \hat{\mathbb{C}} + \omega\hat{\mathbb{A}} = \begin{bmatrix} \mathbf{C}^{(1)} & \mathbf{0} & \mathbf{0} & \ldots \\ \mathbf{0} & \mathbf{C}^{(2)} & \mathbf{0} & \ldots \\ \mathbf{0} & \mathbf{0} & \mathbf{C}^{(3)} & \ddots \\ \vdots & \vdots & \ddots & \ddots \end{bmatrix} + \omega \begin{bmatrix} \tilde{A}_{11}\mathbf{I} & \tilde{A}_{12}\mathbf{I} & \tilde{A}_{13}\mathbf{I} & \ldots \\ \tilde{A}_{21}\mathbf{I} & \tilde{A}_{22}\mathbf{I} & \tilde{A}_{23}\mathbf{I} & \ldots \\ \tilde{A}_{31}\mathbf{I} & \tilde{A}_{32}\mathbf{I} & \tilde{A}_{33}\mathbf{I} & \ldots \\ \vdots & \vdots & \vdots & \ddots \end{bmatrix},$$

$$(17.5)$$

where $\hat{\mathbb{C}} = \mathrm{diag}[\mathbf{C}^{(1)}, \ldots, \mathbf{C}^{(T)}]$ and $\hat{\mathbb{A}} = \tilde{A} \otimes \mathbf{I}$ is the Kronecker product of $\tilde{A}$ and $\mathbf{I}$.

Table 17.1 Summary of our mathematical notation for objects with different dimensions

Typeface	Class	Dimension
$\mathbb{M}$	Matrix	$NT \times NT$
$\mathbf{M}$	Matrix	$N \times N$
M	Matrix	$T \times T$
$\mathbb{v}$	Vector	$NT \times 1$
$\mathbf{v}$	Vector	$N \times 1$
v	Vector	$T \times 1$
M_{ij}	Scalar	1
v_i	Scalar	1

For layer t, the matrix $\mathbf{C}^{(t)}$ can be any matrix whose dominant eigenvector is of interest. In our discussion, we focus on PageRank centrality matrices (see Definition 17.4), but one can alternatively choose eigenvector centrality (Bonacich 1972), hub and authority centralities (Kleinberg 1999), or something else.

The $NT \times NT$ supracentrality matrix $\mathbb{C}(\omega)$ encodes the effects of two distinct types of connections: the layer-specific centrality entries $\{C_{ij}^{(t)}\}$ in the diagonal blocks relate centralities between nodes in layer t; and entries in the off-diagonal blocks encode coupling between layers. The matrix $\hat{\mathbb{A}} = \tilde{A} \otimes \mathbf{I}$ implements uniform and diagonal coupling. The matrix $\mathbf{I}$ encodes diagonal coupling; any two layers t and t' are uniformly coupled because all interlayer edges between them have the same weight $\omega \tilde{A}_{tt'}$.

17.3.2 Joint, Marginal, and Conditional Centralities

As we indicated earlier, we study the dominant right-eigenvalue equation for supracentrality matrices. That is, we solve the eigenvalue equation

$$\mathbb{C}(\omega)\mathbb{v}(\omega) = \lambda_{\max}(\omega)\mathbb{v}(\omega) \,, \tag{17.6}$$

and we interpret entries in the dominant right eigenvector $\mathbb{v}(\omega)$ as scores that measure the importances of node-layer pairs $\{(i, t)\}$. Because the vector $\mathbb{v}(\omega)$ has a block form—its first N entries encode the joint centralities for layer $t = 1$, its next N entries encode the joint centralities for layer $t = 2$, and so on—it is useful to reshape $\mathbb{v}(\omega)$ into a matrix.

Definition 17.6 (*Joint Centrality of a Node-Layer Pair* (Taylor et al. 2017)) Let $\mathbb{C}(\omega)$ be a supracentrality matrix given by Definition 17.5, and let $\mathbb{v}(\omega)$ be its dominant right eigenvector. We encode the *joint centrality* of node i in layer t via the $N \times T$ matrix $\mathbf{W}(\omega)$ with entries

$$W_{it}(\omega) = \mathbb{v}_{N(t-1)+i}(\omega) \,. \tag{17.7}$$

We refer to $W_{it}(\omega)$ as a 'joint centrality' because it reflects the importance of both node i and layer t.

Definition 17.7 (*Marginal Centralities of Nodes and Layers* (Taylor et al. 2017)) Let $\mathbf{W}(\omega)$ encode the joint centralities given by Definition 17.6. We define the *marginal layer centrality* (MLC) and *marginal node centrality* (MNC), respectively, by

$$x_t(\omega) = \sum_i W_{it}(\omega) \,,$$
$$\hat{x}_i(\omega) = \sum_t W_{it}(\omega) \,. \tag{17.8}$$

Definition 17.8 (*Conditional Centralities of Nodes and Layers* (Taylor et al. 2017))
Let $\{W_{it}(\omega)\}$ be the joint centralities given by Definition 17.6; and let $\{x_t(\omega)\}$ and $\{\hat{x}_i(\omega)\}$, respectively, be the marginal layer and node centralities given by Definition 17.7. We define the *conditional centralities* of nodes and layers by

$$Z_{it}(\omega) = W_{it}(\omega)/x_t(\omega),$$
$$\hat{Z}_{it}(\omega) = W_{it}(\omega)/\hat{x}_i(\omega), \tag{17.9}$$

where $Z_{it}(\omega)$ gives the centrality of node i conditioned on layer t and $\hat{Z}_{it}(\omega)$ gives the centrality of layer t conditioned on node i. The quantity $Z_{it}(\omega)$ indicates the importance of node i relative just to the other nodes in layer t.

We ensure that the supracentralities are well-defined (i.e., unique, positive, and finite) with the following theorem.

Theorem 17.1 (Uniqueness and Positivity of Supracentralities (Taylor et al. 2021))
Let $\mathbb{C}(\omega)$ be a supracentrality matrix given by Eq. (17.5). Additionally, suppose that $\tilde{A}$ is an adjacency matrix for a strongly connected graph and that $\sum_t \mathbf{C}^{(t)}$ is an irreducible, nonnegative matrix. It then follows that $\mathbb{C}(\omega)$ is irreducible, nonnegative, and has a simple largest positive eigenvalue $\lambda_{\max}(\omega)$, with corresponding left eigenvector $\mathtt{u}(\omega)$ and right eigenvector $\mathtt{v}(\omega)$ that are each unique and positive. The centralities $\{W_{it}(\omega)\}$, $\{x_i(\omega)\}$, $\{\hat{x}_t(\omega)\}$, $\{Z_{it}(\omega)\}$, and $\{\hat{Z}_{it}(\omega)\}$ are then positive and finite. If we also assume that $\mathbb{C}(\omega)$ is aperiodic, it follows that $\lambda_{\max}(\omega)$ is a unique dominant eigenvalue.

In Fig. 17.2, we show the joint and marginal centralities for the network in Fig. 17.1a. We have normalized the vector $\mathtt{v}(\omega)$ using the 1-norm.

	layer index						
	1	**2**	**3**	**4**	**5**	**6**	**MNC**
1	0.0305	0.0461	0.0493	0.0460	0.0360	0.0195	0.2272
2	0.0198	0.0368	0.0480	0.0501	0.0471	0.0308	0.2326
3	0.0249	0.0491	0.0592	0.0520	0.0402	0.0212	0.2466
4	0.0238	0.0465	0.0660	0.0744	0.0552	0.0275	0.2935
MLC	0.0990	0.1784	0.2225	0.2225	0.1784	0.0990	

(row labels under **node index**)

Fig. 17.2 Joint centralities $\{W_{it}(\omega)\}$ of Definition 17.6 (white cells), with corresponding marginal layer centralities (MLCs) $\{x_t(\omega)\}$ and marginal node centralities (MNCs) $\{\hat{x}_i(\omega)\}$ from Definition 17.7 (gray cells), for the network in panel **a** of Fig. 17.1 with $\omega = 1$. The centrality matrices of the layers are PageRank centrality matrices (see Eq. (17.3)) with a node-teleportation parameter of $\sigma = 0.85$

17.4 Application to a Ph.D. Exchange Network

We apply our supracentrality framework to study centrality trajectories for a temporal network that encodes the graduation and hiring of mathematicians between $N = 231$ mathematical-sciences doctoral programs in the United States during the years 1946–2010 (Taylor et al. 2017). Each edge $A_{ij}^{(t)}$ of the temporal network encodes the number of Ph.D. recipients who graduated from university j in year t and subsequently supervised a Ph.D. student at university i. The edge directions, where $A_{ij}^{(t)}$ is an edge from university i to university j, point in the opposite direction to the flow of people who earn their Ph.D. degrees. We define edge directions in this way to indicate that university i effectively selects the output of university j when hiring someone who received their Ph.D. from university j (Burris 2004; Myers et al. 2011; Clauset et al. 2015). With this convention for the direction of edges, $\{\mathbf{C}^{(t)}\}$ encodes the PageRank matrices of the layers; the highest-ranking universities are the ones that are good sources for the flow of Ph.D. recipients. The network, which we constructed using data from the Mathematics Genealogy Project (2009), is available at Taylor (2019).

We focus our discussion on five universities: Harvard, Massachusetts Institute of Technology (MIT), Princeton, Stanford, and University of California, Berkeley (UC Berkeley). They have the largest PageRank centralities (using a node-teleportation parameter of $\sigma = 0.85$) for a temporally aggregated network with adjacency matrix $\sum_t A^{(t)}$. In all of our experiments, we assume that the layers' centrality matrices are given by PageRank matrices (17.3). As in our other explorations (Taylor et al. 2017, 2021), we vary the interlayer-coupling strength ω to adjust how rapidly centralities change with time. In the present work, our primary focus is investigating the effects on supracentralities of undirected and directed interlayer coupling. See Eqs. (17.1) and (17.2) for the definitions of these interlayer-coupling schemes, and see Fig. 17.1 for visualizations of these two types of interlayer coupling.

We first consider undirected interlayer coupling, so we define $\tilde{A}$ by Eq. (17.1). In Fig. 17.3, we plot the joint and conditional centralities for the five universities. The columns show results for interlayer-coupling strengths $\omega \in \{1, 10, 10^2, 10^3\}$. In the bottom row, we see that progressively larger values of ω yield progressively smoother conditional-centrality trajectories. In the top row, we observe that as one increases ω, the joint centrality appears to limit to one arc of a sinusoidal curve. We prove this result in Sect. 17.5. The most striking results appear in the bottom row of the third column. Based on conditional node centrality, we see that MIT becomes the top-ranked university in the 1950s and then remains so in our data set. Stanford and UC Berkeley gradually develop larger conditional centralities over the 64 years in the data set, whereas the conditional centralities of Princeton and Harvard decrease gradually over this period. The conditional centralities of these five universities are in the top-10 values among all universities in all years of the data set. This is consistent with our results in Taylor et al. (2017, 2021).

We now examine directed interlayer coupling, and we let $\tilde{A}$ encode a directed chain with layer teleportation. See Eq. (17.2) for the specific formula and the bottom row of Fig. 17.1 for an associated visualization. In each panel of Fig. 17.4, we
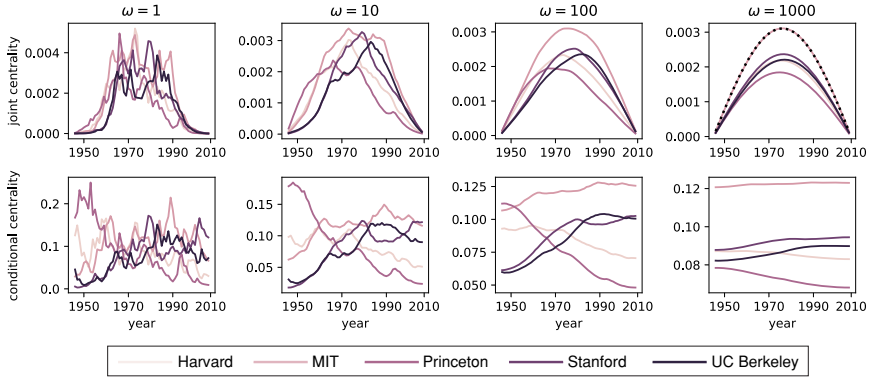
Fig. 17.3 Trajectories of node centralities using undirected interlayer coupling for mathematical-sciences Ph.D. programs at five top universities. The top and bottom rows illustrate joint centralities and conditional node centralities, respectively, that we compute with PageRank centrality matrices with a node-teleportation parameter of $\sigma = 0.85$ and undirected interlayer-adjacency matrix $\tilde{A}$ given by Eq. (17.1) with $\omega \in \{1, 10, 100, 1000\}$. The dotted black curve in the rightmost top panel is the result of an asymptotic approximation that we present in Sect. 17.5

plot the joint centralities and conditional node centralities. The columns give results for interlayer-coupling strengths $\omega \in \{0.1, 1, 10, 100\}$, and the three panels indicate different layer-teleportation probabilities: (a) $\gamma = 0.0001$; (b) $\gamma = 0.001$; and (c) $\gamma = 0.01$. The dotted black curves in the rightmost column indicate large-ω asymptotic approximations that we will present in Sect. 17.5.

To understand the main effect of directed interlayer coupling, we first compare the joint centralities in Fig. 17.4 to those in Fig. 17.3. To help our discussion, we focus on the rightmost column of the two figures. We observe that the joint-centrality trajectories tend to decay with time for directed interlayer coupling, whereas they have peaks and attain their largest values near $t = 1978$ for undirected interlayer coupling. Therefore, directed interlayer coupling tends to "boost" the joint centralities of earlier time layers in comparison to undirected coupling. Comparing panels a–c of Fig. 17.4 (and again focusing on the rightmost column), we observe that the decay is fastest for $\gamma = 0.0001$ (panel a) and slowest for $\gamma = 0.01$ (panel c).

The conditional centralities are also affected by directed interlayer coupling. Consider $\omega = 10$ in Fig. 17.3, and observe that the conditional centrality of Princeton decreases monotonically with time. By contrast, observe in Fig. 17.4a,b for $\omega = 10$ that the conditional centrality of Princeton now decreases between $t = 1946$ and about $t = 1988$, but then it increases.

For our last experiment, we examine how reversing the direction of the interlayer edges changes the results of our supracentrality calculations. We repeat the previous experiment with directed interlayer edges, except that we set $\tilde{A}$ to be the transpose of the matrix that we defined by Eq. (17.2). One motivation is that for some applications, the most recent time layers are more important than the earliest time layers. One can incorporate this idea into our supracentrality framework by reversing the direction of the interlayer edges. In Fig. 17.5, we plot the same quantities as in Fig. 17.4, except
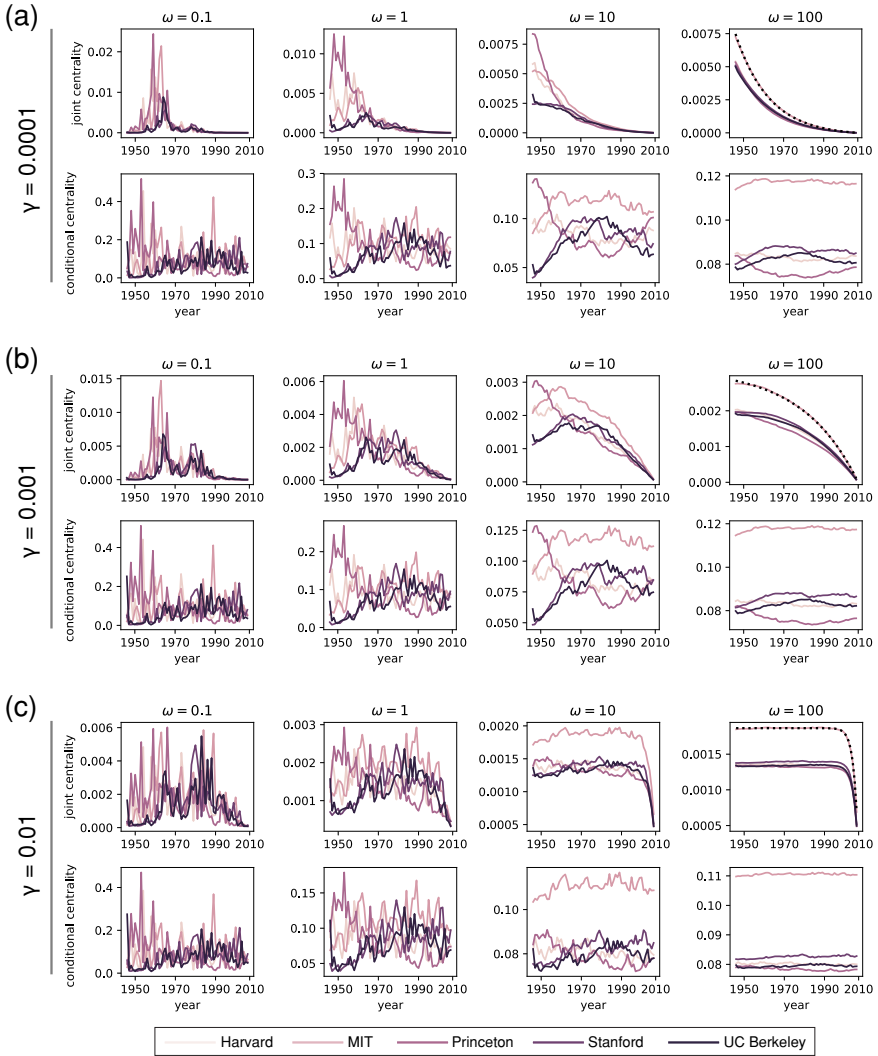
Fig. 17.4 Trajectories of node centralities using directed interlayer coupling for mathematical-sciences Ph.D. programs at five top universities. This figure is similar to Fig. 17.3, except that the interlayer-adjacency matrix $\tilde{A}$ is now given by Eq. (17.2), which corresponds to a directed chain with layer teleportation with probability γ. Panels **a**, **b**, and **c** show results for $\gamma = 0.0001$, $\gamma = 0.001$, and $\gamma = 0.01$, respectively. The dotted black curves in the rightmost top subpanels of panels **a**–**c** are results of an asymptotic approximation that we present in Sect. 17.5. For sufficiently large ω and sufficiently small γ, the joint centralities decrease with time

that now we take the directed interlayer edges to have the opposite direction (so we have reversed the arrow of time). Observe that the joint centralities now tend to increase with time; by contrast, in Fig. 17.4, they tend to decrease with time. These trends are most evident in the rightmost columns. We also observe differences in the conditional centralities. For example, focusing on $\omega = 10$ in the third column of Fig. 17.5, we see that Princeton never has the largest conditional centrality. By contrast, for $\omega = 10$ in Figs. 17.3 and 17.4a,b, Princeton has the largest conditional centrality for the earliest time steps (specifically, for $t \in \{1946, \ldots, 1954\}$).

Understanding how the weights, topologies, and directions of interlayer coupling affect supracentralities is essential to successfully deploying supracentrality analysis to reveal meaningful insights. The above experiments highlight that one can tune the weights and topology of interlayer coupling to emphasize either earlier or later time layers. Specifically, one can adjust the parameters ω and γ, as well as the direction of the interlayer edges, to cater a study to particular data sets and particular research questions. In our investigation in this section, we considered both the case in which $\tilde{A}$ is given by Eq. (17.2) and the case in which it is given by the transpose of the matrix that we determine from Eq. (17.2). It is worth considering how these different choices of interlayer edge directions are represented in the supracentrality matrix $\mathbb{C}(\omega)$ and the consequences of these choices. Specifically, each layer's PageRank matrix $\mathbf{C}^{(t)}$ is defined in Eq. (17.3) using the transpose of the layer's adjacency matrix $\mathbf{A}^{(t)}$, yet when coupling the centrality matrices, we do not take the transpose of $\tilde{A}$ when defining $\mathbb{C}(\omega)$ in Eq. (17.5). Accordingly, one may worry that the matrix $\mathbb{C}(\omega)$ effectively acts in the forward direction for the intralayer edges but in the opposite direction for the interlayer edges. However, this does not lead to any inherent contradiction, as the meanings of the directions of these two types of edges are fundamentally different. The direction of the intralayer edges dictates the flow of random walkers, whereas the direction of the interlayer edges couples the centralities of the different layers. In other applications, it may be necessary to encode the directions of the interlayer and intralayer edges in the same way, but there is no reason why one cannot encode the directions of interlayer and intralayer edges in different ways in a supracentrality formalism. As we have demonstrated by considering both $\tilde{A}$ and its transpose—and thus by treating the effect of the interlayer edges in opposite ways in these two calculations—both uses are meaningful. They also probe different aspects of temporal data.

17.5 Asymptotic Behavior for Small and Large Interlayer-Coupling Strength ω

In this section, we summarize the asymptotic results from Taylor et al. (2021) that reveal the behavior of supracentralities in the limit of small and large ω. In our present discussion, we focus on dominant right eigenvectors.
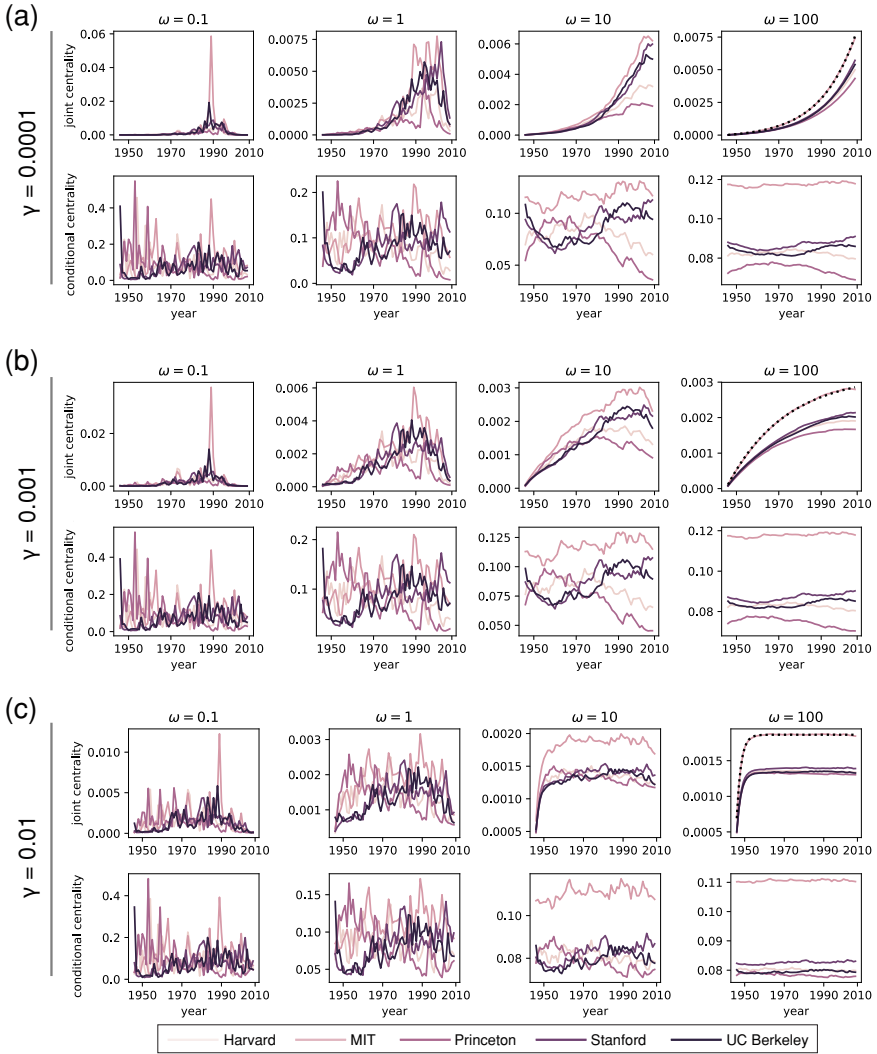
Fig. 17.5 Trajectories of node centralities using reversed directed interlayer coupling for mathematical-sciences Ph.D. programs at five top universities. This figure is identical to Fig. 17.4, except that $\tilde{A}$ is now given by the transpose of the matrix from Eq. (17.2), such that the directed chain points backwards in time. For sufficiently large ω and sufficiently small γ, the joint centralities now increase with time

To motivate our asymptotic analysis, consider the top-right subpanels in each panel of Figs. 17.3, 17.4, and 17.5. In each of these subpanels, we plot (in dotted black curves) the results of an asymptotic analysis of the dominant right eigenvector $\tilde{\mathbf{v}}^{(1)}$ of $\tilde{A}$ for the joint centrality of MIT in the limit of large ω. We observe excellent agreement with our numerical calculations. Therefore, for sufficiently large ω, one can understand the effects of both undirected and directed interlayer couplings (as encoded in an interlayer-adjacency matrix $\tilde{A}$) by examining the dominant right eigenvector of $\tilde{A}$. For large values of ω, this eigenvector captures the limit of the joint centralities as a function with a peak for undirected coupled (see Fig. 17.3), decay in time for directed coupling (see Fig. 17.4), and growth in time for directed coupling when reversing the arrow of time (see Fig. 17.5).

17.5.1   Layer Decoupling in the Limit of Small ω

We begin with some notation. Let $\tilde{\mu}_1$ be the dominant eigenvalue (which we assume to be simple) of $\tilde{A}$, and let $\tilde{\mathbf{u}}^{(1)}$ and $\tilde{\mathbf{v}}^{(1)}$ denote its corresponding left and right eigenvectors. Given a set $\{\mathbf{C}^{(t)}\}$ of centrality matrices, we let $\mu_1^{(t)}$ be the dominant eigenvalue (which we also assume to be simple) of $\mathbf{C}^{(t)}$; the vectors $\mathbf{u}^{(1,t)}$ and $\mathbf{v}^{(1,t)}$ are the corresponding left and right eigenvectors. Let $\{\mu_1^{(t)}\}$ denote the set of spectral radii, where $\lambda_{\max}(0) = \max_t \mu_1^{(t)}$ is the maximum eigenvalue over all layers. (Recall that $\lambda_{\max}(\omega)$ is the dominant eigenvalue of the supracentrality matrix $\mathbb{C}(\omega)$.) Let $\mathscr{P} = \{t : \mu_1^{(t)} = \lambda_{\max}(0)\}$ denote the set of layers whose centrality matrices have an eigenvalue that achieves the maximum. When the layers' centrality matrices $\{\mathbf{C}^{(t)}\}$ are PageRank matrices given by Eq. (17.3), it follows that $\mu_1^{(t)} = 1$ for all t (i.e., $\mathscr{P} = \{1, \ldots, T\}$), the corresponding left eigenvector is $\mathbf{u}^{(1,t)} = [1, \ldots, 1]^T/N$, and $\mathbf{v}^{(1,t)}$ is the PageRank vector for layer t. Furthermore, for each t, we define the length-NT "block" vector $\mathbb{v}^{(1,t)} = \mathbf{e}^{(t)} \otimes \mathbf{v}^{(1,t)}$, which consists of zeros in all blocks except for block t, which equals $\mathbf{v}^{(1,t)}$. The vector $\mathbf{e}^{(t)}$ is a length-T unit vector that consists of zeros in all entries except for entry t, which is 1.

We now present a theorem from Taylor et al. (2021), although we restrict our attention to the part of it that pertains to the right dominant eigenvector.

Theorem 17.2 (Weak-Coupling Limit of Dominant Right Eigenvectors (Taylor et al. 2021)) *Let $\mathbb{v}(\omega)$ be the dominant right eigenvector of a supracentrality matrix that is normalized using the 1-norm and satisfies the assumptions of Theorem 17.1. Additionally, let $\mathscr{P} = \{t : \mu_1^{(t)} = \lambda_{\max}(0)\}$ denote the set of indices associated with the eigenvalues of $\mathbf{C}^{(t)}$ that equal the largest eigenvalue $\lambda_{\max}(0)$ of $\mathbb{C}(0)$. We assume that each layer's dominant eigenvalue $\mu_1^{(t)}$ is simple. It then follows that the $\omega \to 0^+$ limit of $\mathbb{v}(\omega)$ satisfies*

$$\mathbb{v}(\omega) \to \sum_{t \in \mathscr{P}} \alpha_t \mathbb{v}^{(1,t)} , \tag{17.10}$$

where the vector $\boldsymbol{\alpha} = [\alpha_1, \ldots, \alpha_T]^T$ has nonnegative entries and is the unique solution of the dominant eigenvalue equation

$$X\boldsymbol{\alpha} = \lambda_1 \boldsymbol{\alpha} \,. \tag{17.11}$$

The eigenvalue λ_1 needs to be determined, and the entries of X are

$$X_{tt'} = \tilde{A}_{t,t'} \frac{\langle \mathbf{u}^{(1,t)}, \mathbf{v}^{(1,t')} \rangle}{\langle \mathbf{u}^{(1,t)}, \mathbf{v}^{(1,t)} \rangle} \chi(t)\chi(t') \,, \tag{17.12}$$

where $\chi(t) = \sum_{t' \in \mathscr{P}} \delta_{tt'}$ is an indicator function: $\chi(t) = 1$ if $t \in \mathscr{P}$ and $\chi(t) = 0$ otherwise. The vector $\boldsymbol{\alpha}$ must also be normalized to ensure that the right-hand side of Eq. (17.10) is normalized (by setting $\|\boldsymbol{\alpha}\|_p = 1$ for normalization using a p-norm).

17.5.2 Layer Aggregation in the Limit of Large ω

To study the $\omega \to \infty$ limit, it is convenient to divide Eq. (17.6) by ω and define $\varepsilon = 1/\omega$ to obtain

$$\tilde{\mathbb{C}}(\varepsilon) = \varepsilon \mathbb{C}(\varepsilon^{-1}) = \varepsilon\hat{\mathbb{C}} + \hat{\mathbb{A}} \,, \tag{17.13}$$

which has right eigenvectors $\tilde{\mathbb{v}}(\varepsilon)$ that are identical to those of $\mathbb{C}(\omega)$ (specifically, $\tilde{\mathbb{v}}(\varepsilon) = \mathbb{v}(\varepsilon^{-1})$). Its eigenvalues $\{\tilde{\lambda}_i\}$ are scaled by ε, so $\tilde{\lambda}_i(\varepsilon) = \varepsilon\lambda_i(\varepsilon^{-1})$.

Before presenting results from Taylor et al. (2021), we define a few additional concepts. Let $\tilde{\mathbb{v}}^{(1,j)} = \tilde{\mathbf{e}}^{(j)} \otimes \tilde{\boldsymbol{v}}^{(1)}$ denote a block vector that consists of zeros in all blocks except for block j, which equals the dominant right eigenvector $\tilde{\boldsymbol{v}}^{(1)}$ of $\tilde{A}$. The vector $\tilde{\mathbf{e}}^{(j)}$ is a length-N unit vector that consists of zeros in all entries except for entry j, which is 1. We also define the stride permutation matrix

$$\mathbb{P}_{kl} = \begin{cases} 1\,, & l = \lceil k/N \rceil + T\,[(k-1) \bmod N] \\ 0\,, & \text{otherwise}\,, \end{cases} \tag{17.14}$$

where the ceiling function $\lceil \theta \rceil$ denotes the smallest integer that is at least θ and 'mod' denotes the modulus function (i.e., $a \bmod b = a - b\lceil a/b - 1 \rceil$).

Theorem 17.3 (Strong-Coupling Limit of Dominant Eigenvectors (Taylor et al. 2021)) *Let $\tilde{A}$, $\tilde{\mu}_1$, $\tilde{\boldsymbol{u}}^{(1)}$, and $\tilde{\boldsymbol{v}}^{(1)}$ be defined as above, with the same assumptions as in Theorem 17.1. It then follows that the dominant eigenvalue $\tilde{\lambda}_{\max}(\varepsilon)$ and the associated eigenvector $\mathbb{v}(\varepsilon)$ of $\mathbb{C}(\varepsilon)$ converge as $\varepsilon \to 0^+$ to the following expressions:*

$$\tilde{\lambda}_{\max}(\varepsilon) \to \tilde{\mu}_1 \,,$$

$$\tilde{\mathbb{v}}(\varepsilon) \to \sum_j \tilde{\alpha}_j \mathbb{P} \tilde{\mathbb{v}}^{(1,j)} \,, \tag{17.15}$$

where the constants $\{\tilde{\alpha}_i\}$ solve the dominant eigenvalue equation

$$\tilde{\mathbf{X}} \tilde{\boldsymbol{\alpha}} = \tilde{\mu}_1 \tilde{\boldsymbol{\alpha}} \,, \tag{17.16}$$

with

$$\tilde{X}_{ij} = \sum_t C_{ij}^{(t)} \frac{\tilde{u}_t^{(1)} \tilde{v}_t^{(1)}}{\langle \tilde{\boldsymbol{u}}^{(1)}, \tilde{\boldsymbol{v}}^{(1)} \rangle} \,. \tag{17.17}$$

We normalize the vector $\tilde{\boldsymbol{\alpha}}$ to ensure that the right-hand side of Eq. (17.15) is normalized.

Equation (17.17) indicates that the strong-coupling limit effectively aggregates the centrality matrices $\{\mathbf{C}^{(t)}\}$ across time via a weighted average, with weights that depend on the dominant left and right eigenvectors of $\tilde{A}$. When $\tilde{A}$ encodes an undirected chain (see Eq. (17.1) and the top row of Fig. 17.1), it follows that (Taylor et al. 2017)

$$\tilde{\mathbf{X}} = \sum_t \mathbf{C}^{(t)} \frac{\sin^2\left(\frac{\pi t}{T+1}\right)}{\sum_{t=1}^T \sin^2\left(\frac{\pi t}{(T+1)}\right)} \,. \tag{17.18}$$

The dotted black curve in the top-right subpanel of Fig. 17.3 shows a scaled version of $\tilde{\boldsymbol{v}}^{(1)}$, which is defined by the normalized sinusoidal weightings in Eq. (17.18). The dotted black curves in the top-right subpanels of each panel of Figs. 17.4 and 17.5 also show $\tilde{\boldsymbol{v}}^{(1)}$ (with $\tilde{A}$ given by Eq. (17.2) and by the transpose of the matrix that we obtain from Eq. (17.2), respectively), which we scale to normalize the joint centralities.

17.6　Discussion

We presented a supracentrality framework to study how the importances of the nodes of a temporal network change with time. Our approach involves representing a temporal sequence of networks as time layers of a multiplex network and using the strength and topology of coupling between time layers to tune centrality trajectories. A key feature of our approach is that it simultaneously yields the centralities of all nodes at all times by computing the dominant right eigenvector of a supracentrality matrix.

Inspired by ideas from probability theory, we examined three types of eigenvector-based supracentralities:

  (i) the joint centrality of a node-layer pair (i, t); this captures the combined importance of node i and time layer t;

 (ii) the marginal centrality of a node i or time t; these capture separate importances of a node or a time layer; and

(iii) the conditional centrality of a node i at time t; this captures the importance of a node relative only to other nodes at that particular time.

    Because our approach involves analyzing the dominant eigenvector of a centrality matrix, it generalizes eigenvector-based centralities, such as PageRank, hub and authority centralities, and (vanilla) eigenvector centrality. Naturally, it is desirable to extend supracentralities to analyze networks that are both temporal and multiplex (Kivelä et al. 2014). Another important generalization of centrality analysis is the study of continuous-time temporal networks and streaming network data (Grindrod and Higham 2014; Ahmad et al. 2021), and it will be insightful to extend supracentralities to such situations.

References

W. Ahmad, M.A. Porter, M. Beguerisse-Díaz, IEEE Trans. Netw. Sci. Eng. **8**(2), 1759 (2021)

A. Alsayed, D.J. Higham, Chaos, Solitons Fractals **72**, 35 (2015)

F. Arrigo, D.J. Higham, Appl. Netw. Sci. **2**(1), 17 (2017)

D.S. Bassett, M.A. Porter, N.F. Wymbs, S.T. Grafton, J.M. Carlson, P.J. Mucha, Chaos **23**(1), 013142 (2013)

F. Battiston, V. Nicosia, V. Latora, Phys. Rev. E **89**(3), 032804 (2014)

C.T. Bergstrom, J.D. West, M.A. Wiseman, J. Neurosci. **28**(45), 11433 (2008)

P. Bonacich, J. Math. Sociol. **2**(1), 113 (1972)

S.P. Borgatti, C. Jones, M.G. Everett, Connections **21**(2), 27 (1998)

S. Brin, L. Page, in *Proceedings of the Seventh International World Wide Web Conference* (1998), pp. 107–117

V. Burris, Am. Sociol. Rev. **69**(2), 239 (2004)

T. Callaghan, M.A. Porter, P.J. Mucha, Am. Math. Mon. **114**(9), 761 (2007)

T. Chakraborty, R. Narayanam, in *2016 IEEE 32nd International Conference on Data Engineering (ICDE)* (IEEE, Piscataway, 2016), pp. 397–408

T.P. Chartier, E. Kreutzer, A.N. Langville, K.E. Pedings, SIAM J. Sci. Comput. **33**(3), 1077 (2011)

I. Chen, M. Benzi, H.H. Chang, V.S. Hertzberg, J. Complex Netw. **5**(2), 274 (2016)

A. Clauset, S. Arbesman, D.B. Larremore, Sci. Adv. **1**(1), e1400005 (2015)

M. De Domenico, A. Solé-Ribalta, E. Cozzo, M. Kivelä, Y. Moreno, M.A. Porter, S. Gómez, A. Arenas, Phys. Rev. X **3**(4), 041022 (2013)

D.R. DeFord, *in International Workshop on Complex Networks and their Applications* (Springer, Berlin, 2017), pp.1111–1123

D.R. DeFord, S.D. Pauls, J. Complex Netw. **6**(3), 353 (2017)

C. Ding, K. Li, Neurocomputing **312**, 263 (2018)

E. Estrada, Phys. Rev. E **88**(4), 042811 (2013)

K. Faust, Soc. Netw. **19**(2), 157 (1997)

C. Fenu, D.J. Higham, SIAM J. Matrix Anal. Appl. **38**(2), 343 (2017)

J. Flores, M. Romance, J. Comput. Appl. Math. **330**, 1041 (2018)

J.H. Fowler, S. Jeon, Soc. Netw. **30**(1), 16 (2008)

J.H. Fowler, T.R. Johnson, J.F. Spriggs II, S. Jeon, P.J. Wahlbeck, Policy Anal. **15**(3), 324 (2007)

D.F. Gleich, SIAM Rev. **57**(3), 321 (2015)

P. Grindrod, D.J. Higham, SIAM Rev. **55**(1), 118 (2013)

P. Grindrod, D.J. Higham, Proc. R. Soc. A **470**(2165), 20130835 (2014)

P. Grindrod, M.C. Parsons, D.J. Higham, E. Estrada, Phys. Rev. E **83**(4), 046120 (2011)

R. Guimerà, S. Mossa, A. Turtschi, L.A.N. Amaral, Proc. Natl. Acad. Sci. U. S. A. **102**(22), 7794 (2005)

A. Halu, R.J. Mondragón, P. Panzarasa, G. Bianconi, PLoS ONE **8**(10), e78293 (2013)

P. Holme, Adv. Complex Syst. **6**(2), 163 (2003)

P. Holme, Eur. Phys. J. B **88**(9), 234 (2015)

P. Holme, J. Saramäki, Phys. Rep. **519**(3), 97 (2012)

P. Holme, J. Saramäki (eds.), *Temporal Networks* (Springer, Berlin, 2013)

D.W. Huang, Z.G. Yu, Sci. Rep. **7**, 41454 (2017)

Q. Huang, C. Zhao, X. Zhang, X. Wang, D. Yi, Europhys. Lett. **118**(3), 36001 (2017)

H. Jeong, S.P. Mason, A.L. Barabási, Z.N. Oltvai, Nature **411**(6833), 41 (2001)

D. Kempe, J. Kleinberg, É. Tardos, in *Proceedings of the Ninth ACM SIGKDD International Conference on Knowledge Discovery and Data Mining* (ACM, New York, 2003), pp. 137–146

H. Kim, J. Tang, R. Anderson, C. Mascolo, Comput. Netw. **56**(3), 983 (2012)

M. Kivelä, A. Arenas, M. Barthelemy, J.P. Gleeson, Y. Moreno, M.A. Porter, J. Complex Netw. **2**(3), 203 (2014)

J. Kleinberg, J. ACM **46**(5), 604 (1999)

G. Kossinets, J. Kleinberg, D. Watts, in *Proceedings of the 14th ACM SIGKDD International Conference on Knowledge Discovery and Data Mining* (ACM, New York, 2008), pp. 435–443

V. Kostakos, Phys. A **388**(6), 1007 (2009)

A.N. Langville, C.D. Meyer, *Google's PageRank and Beyond: The Science of Search Engine Rankings* (Princeton University Press, Princeton, 2006)

E.A. Leicht, G. Clarkson, K. Shedden, M.E.J. Newman, Eur. Phys. J. B **59**(1), 75 (2007)

K. Lerman, R. Ghosh, J.H. Kang, in *Proceedings of the Eighth Workshop on Mining and Learning with Graphs* (ACM, New York, 2010), pp. 70–77

H. Liao, M.S. Mariani, M. Medo, Y.C. Zhang, M.Y. Zhou, Phys. Rep. **689**, 1 (2017)

M. Magnani, B. Micenkova, L. Rossi, arXiv preprint arXiv:1303.4986 (2013)

M. Magnani, L. Rossi, in *2011 International Conference on Advances in Social Networks Analysis and Mining (ASONAM)* (IEEE, Piscataway, 2011), pp. 5–12

M.S. Mariani, M. Medo, Y.C. Zhang, Sci. Rep. **5**, 16181 (2015)

M.S. Mariani, M. Medo, Y.C. Zhang, J. Informetr. **10**(4), 1207 (2016)

N. Masuda, M.A. Porter, R. Lambiotte, Phys. Rep. **716–717**, 1 (2017)

S. Motegi, N. Masuda, Sci. Rep. **2**, 904 (2012)

P.J. Mucha, M.A. Porter, Chaos **20**(4), 041108 (2010)

S.A. Myers, P.J. Mucha, M.A. Porter, Chaos **21**(4), 041104 (2011)

M.E.J. Newman, *Networks*, 2nd edn. (Oxford University Press, Oxford, 2018)

M.K.P. Ng, X. Li, Y. Ye, in *Proceedings of the 17th ACM SIGKDD International Conference on Knowledge Discovery and Data Mining* (ACM, New York, 2011), pp. 1217–1225

L. Page, S. Brin, R. Motwani, T. Winograd, The PageRank citation ranking: Bringing order to the Web. Technical Report 1999-66. Stanford InfoLab (1999)

A.R. Pamfil, S.D. Howison, R. Lambiotte, M.A. Porter, SIAM J. Math. Data Sci. **1**(4), 667 (2019)

R. Pan, J. Saramäki, Phys. Rev. E **84**(1), 016105 (2011)

M.A. Porter, Not. Am. Math. Soc. **65**(11), 1419 (2018)

S. Praprotnik, V. Batagelj, Ars Mat. Contemp. **11**(1), 11 (2015)

C. Rahmede, J. Iacovacci, A. Arenas, G. Bianconi, J. Complex Netw. **6**(5), 733 (2017)

R.A. Rossi, D.F. Gleich, *Algorithms and Models for the Web Graph* (Springer, Berlin, 2012), pp.126–137

S. Saavedra, S. Powers, T. McCotter, M.A. Porter, P.J. Mucha, Phys. A **389**(5), 1131 (2010)

L. Solá, M. Romance, R. Criado, J. Flores, A.G. del Amo, S. Boccaletti, Chaos **23**(3), 033131 (2013)

A. Solé-Ribalta, M. De Domenico, S. Gómez, A. Arenas, in *Proceedings of the 2014 ACM Conference on Web Science* (ACM, New York, 2014), pp. 149–155

A. Solé-Ribalta, M. De Domenico, S. Gómez, A. Arenas, Phys. D **323**, 73 (2016)

C. Spatocco, G. Stilo, C. Domeniconi, arXiv preprint arXiv:1801.08026 (2018)

T. Takaguchi, Y. Yano, Y. Yoshida, Eur. Phys. J. B **89**(2), 1 (2016)

M.Y. Tang, M. Musolesi, C. Mascolo, V. Latora, V. Nicosia, in *Proceedings of the 3rd Workshop on Social Network Systems—SNS '10* (2010), pp. 1–6

S. Tavassoli, K.A. Zweig, *in 2016 Third European Network Intelligence Conference (ENIC)* (IEEE, Piscataway, 2016), pp. 25–32

D. Taylor, Data release: Ph.D. exchange in the Mathematical Genealogy Project. https://sites.google.com/site/danetaylorresearch/data (2019)

D. Taylor, R.S. Caceres, P.J. Mucha, Phys. Rev. X **7**(3), 031056 (2017)

D. Taylor, S.A. Myers, A. Clauset, M.A. Porter, P.J. Mucha, Multiscale Model. Simul. **15**(1), 537 (2017)

D. Taylor, M.A. Porter, P.J. Mucha, Multiscale Model. Simul. **19**(1), 113 (2021)

The Mathematics Genealogy Project. http://www.genealogy.ams.org; data provided 19 October 2009

F. Tudisco, F. Arrigo, A. Gautier, J. SIAM. Appl, Math. **78**(2), 853 (2018)

D. Walker, H. Xie, K.K. Yan, S. Maslov, J. Stat. Mech. **2007**(6), P06010 (2007)

W.H. Weir, S. Emmons, R. Gibson, D. Taylor, P.J. Mucha, Algorithms **10**(3), 93 (2017)

M.J. Williams, M. Musolesi, R. Soc. Open Sci. **3**(6) (2016)

K. You, R. Tempo, L. Qiu, IEEE Trans. Autom. Control **62**(5), 2080 (2017)